CENTRE FOR
SYSTEMS
SCIENCE

LCCR

Simon Fraser University, Burnaby, B.C., Canada V5A 1S6 / (604) 291-4704

92-06718/

Variational Approach to Mutual Illumination in Color Images

Mark S Drew and Brian V Funt

CSS/LCCR TR 90-21

December 1990

Variational Approach to Mutual Illumination in Color Images

Mark S. Drew and Brian V. Funt
School of Computing Science
Simon Fraser University
Vancouver, B.C.
Canada V5A 1S6
(604) 291-4682

Abstract

We propose a variational method for recovering the surface spectral reflectance and the spectral power distribution of the incident illumination from 3-band, color images of surfaces participating in mutual illumination. The color variations caused by mutual illumination, therefore, allow us to establish color constancy. In addition, we show how to recover shading information as well as geometric information about shape and position. The variational integral makes use of finite dimensional linear models for light and surface reflectance and is based on a one-bounce model of interreflection. Tests of the method for simulations of a simple geometry show reasonable accuracy for recovered spectra and for interreflection shape factors.

©1990 M.S. Drew and B.V. Funt

1 Introduction

Interreflection of light plays an important part in the generation of intensities and colors in images. A white ceiling contributes a good deal of the luminance in a room via this physical mechanism, also referred to as mutual reflection [8, 4] or mutual illumination [15, 6, 7, 23].

While study of this phenomenon has a long history in illumination and thermal engineering [17, 24, 25], it has only relatively recently come under consideration in computer vision. One reason is that the problem is inherently nonlinear, in that the mutual illumination impinging on a surface 1 from another surface 2 is in part the result of reflection from surface 2 to surface 1. The seminal work of Koenderink and van Doorn [19] sets out formally this nonlinear problem, for known shapes, and its integral equation formal solution.

References [6, 7, 23] are concerned with the very broad problem of attempting to recover the mutual illumination from an image of a set of surface patches all of which can interreflect and each of which can have albedo that changes within a patch. The emphasis in these papers is on solving for albedo for very general sets of concave surfaces, including ones that are sufficiently concave as to self-reflect and ones that have lines-of-sight blocked by occlusions. Nayar et al. [23] find that shape-from-intensity schemes can succeed even with mutual illumination present if shape calculations are iterated with generation of mutual illumination information.

In computer graphics, the radiosity method [11, 13] addresses the interreflection problem more from an engineering perspective in which the emphasis (see, e.g., [24]) is on finding how large patches (the walls of a room, say) interreflect, where each patch is assumed to have uniform reflectance. Of course both directions, the illumination engineering approach and the more formal approach, can coincide in a proper limit.

The radiosity method replaces albedo by three color bands for representing surface reflectance. From the underlying theory [24], however, it is possible to carry out a diffuse interreflection calculation using a whole spectrum description of surface reflectance. In [8, 4] we calculated the color signal spectrum reflected from a simple geometry illuminated by isotropic illumination, with patches participating in full nonlinear mutual illumination. We found that finite-dimensional model approximations of both surface spectral reflectance and the illumination spectrum could be recovered from a color camera image of this set of patches by using a simple model that assumed multiple bounces from one surface to another could be ignored. As well, we recovered a configuration factor summarizing information on the orientation and shape of the surfaces to a surprising degree of accuracy.

In that work [4] it was necessary to assume that on each patch one could find a spot where mutual illumination could be considered negligible. While this restriction often holds, it represents a serious flaw in the method. For the special case of only two surfaces, we found that by combining color camera RGB values from two such areas far from the mutual reflection edge with values that were measured near the edge we could obtain color constancy — i.e., constant color descriptors of the surface independent of the lighting.

Here we find that the assumption that some spot exists with negligible mutual illumination can be dispensed with provided that one takes into account *all* the information available from all patches. This can be achieved by finding a solution for all the parameters of the image at once by including them in an optimization problem that can be solved using the calculus of variations.

Again we assume that surface reflectance is uniform over each patch, although patch size could in principle be reduced to allow for changing reflectance on each surface. However, we find that it is possible, using this variational method, to allow for a point source of illumination as well as diffuse illumination. This means that the method recovers the shading at each point. The main assumption involved is again the one-bounce approximation. This assumption renders the resulting equations solvable because they can be turned into a set of nonlinear equations to be solved iteratively by solution of intermediate linear equations.

The one-bounce assumption means that the method might not work well for highly concave folds in surfaces or in other regions where mutual illumination dominates. However, we expect the method to work for many ordinary images. Shadows are not included in our analysis.

In Section 2 we outline the finite-dimensional linear models for surface reflectance and illumination on which our method rests. In Section 3 we introduce the variational description of the problem and address the issue of how much interreflection information can be gleaned from an image. In Section 4 we detail the resulting equations for a simplified calculation involving only two convex patches and no shading. Section 5 tests the method by simulating mutual illumination edges composed of planar sides for various materials. The usefulness of this simple geometry is that all properties can be completely determined analytically so that recovered results can be compared with exact values.

We find that the method recovers surface surface spectral reflectance and the illumination spectrum with reasonable accuracy, as well as recovering a good approximation of the interreflection configuration factor, which encapsulates surface geometry information.

2 Finite-Dimensional Models

Natural surface spectral reflectance functions and illumination spectra have been found to be well-modeled by finite-dimensional linear models [22, 21, 26]. Using a set of basis spectral functions E_a, $a = 1..m$ we model illumination $E(\lambda)$ by a sum

$$E(\lambda) \simeq \sum_{a=1}^{m} \epsilon_a \, E_a(\lambda) \, . \tag{1}$$

Let us restrict our attention to Lambertian surfaces. Then we can model surface spectral reflectance $S(\lambda)$ by a similar sum with another basis S_μ, $\mu = 1..n$:

$$S(\lambda) \simeq \sum_{\mu=1}^{n} \sigma_\mu \, S_\mu(\lambda) \, . \tag{2}$$

When light is reflected from a diffuse surface, the resulting spectrum, the *color signal* $C(\lambda)$, is formed via the product

$$C(\lambda) = E(\lambda)\, S(\lambda). \tag{3}$$

Now consider the result of applying a set of filters with response functions $R_k(\lambda)$, $k = 1..s$ to the color signal. For a color camera, $s = 3$. Calling the resulting set of camera or eye responses ρ_k, substituting (1) and (2) into (3) we have [1]

$$\begin{aligned} \rho_k &= \int C(\lambda)\, R_k(\lambda)\, d\lambda \\ &= \sum_{a=1}^{m} \sum_{\mu=1}^{n} \epsilon_a\, \sigma_\mu\, g_{a\mu k} \end{aligned} \tag{4}$$

where [22]

$$g_{a\mu k} \equiv \int E_a(\lambda) S_\mu(\lambda)\, R_k(\lambda)\, d\lambda\,.$$

In the next section we study light formed by one color signal reflecting off the same or another surface. Therefore, we need a matrix similar to $g_{a\mu k}$, but of dimension four. Let

$$h_{a\mu\nu k} \equiv \int E_a(\lambda) S_\mu(\lambda) S_\nu(\lambda)\, R_k(\lambda)\, d\lambda\,.$$

For our illumination basis set we shall adopt that determined by Judd via a principal component analysis of daylight spectra [16]. For surface reflectance, we use either those basis functions given by Cohen [2] by means of a similar analysis of a set of Munsell chips, or else a set of basis vectors found by our own principal component analysis for the set of natural reflectances catalogued by Krinov [20]. For camera filters we use Kodak filters #25 (red), #58 (green) and #47B (blue) shown in [8].

3 Variational Equations

3.1 Assumptions

Consider the configuration of two surfaces depicted in Fig. 1. We suppose the surfaces to be ideal Lambertian reflectors. As well, assume the illumination is composed of two components, diffuse isotropic radiation and a point source (with unknown position) or spatially distributed light source. Then if both components are assumed to have the same spectral function (cf. [10]) the illumination

[1] Indices $a, b, c, \ldots$ for illumination go from 1 to m; greek indices for surface reflectance go from 1 to n; index k for sensor values goes from 1 to s.

$E(\lambda)$ can be approximated as a sum as in Section 2. Because of the point source component, the illumination impinging on a surface point will vary by a shading factor as a result of foreshortening.

We lump both the **diffuse** factor $\equiv 1$ and the shading factor for the point source into a single factor α. With the surface 2-space parameterized by a set of parameters that we denote simply by x, the illumination at a point is

$$E(x,\lambda) = \alpha(x)\, E(\lambda)$$

where we assume $E(\lambda)$ is constant throughout the scene. It is straightforward to extend the model to include two components of illumination having different spectra but we shall not do so here. Nevertheless the variational formulation introduced below can in fact handle such cases.

For Fig. 1 the one-bounce approximation reduces the mutual illumination problem to consideration of light reflected from surface 1 to itself and from surface 2 to surface 1, and similarly for surface 2. For known surfaces, for each type of interreflection one can calculate the sum of all contributions to mutual illumination at a point x. Here we address the inverse problem and seek to derive these contributions. Let the factor β^{21} comprise all reflection from every point on surface 2 to a small area on surface 1. Thus β^{21} lumps all shape, orientation, and shading factors for mutual illumination into one parameter.

3.2 One-bounce color signal

Let us turn now to the general case of many surfaces. Let the image be derived from a configuration with $I = 1..M$ patches, each of which is assumed to have uniform surface reflectance $S^I(\lambda)$. Following [24] we divide each surface patch into many small sub-patches. On the Ith patch (again denoting position simply by x) the one-bounce approximation to the color signal from location x is given by

$$C^I(x,\lambda) = E(x,\lambda)S^I(\lambda) + \sum_{J=1}^{M} \beta^{JI}(x)S^I(\lambda)E(\lambda)S^J(\lambda)\,. \tag{5}$$

In the above, $\beta^{JI}(x)$ is different for every patch pair. In particular, eqn. (5) includes self-reflection.

3.3 Finite-dimensional model RGB equations

We now substitute the finite-dimensional linear model approximations of Section 2 and carry out the integrations of eqn. (4). By straightforward substitution we arrive at camera RGB values

$$\rho_k^I(x) = \alpha^I(x) \sum_{a=1}^{} \sum_{\mu=1}^{} \epsilon_a \sigma_\mu^I\, g_{i\mu k} + \sum_J \beta^{JI}(x) \sum_\mu \sum_a \sum_\nu \sigma_\mu^I \epsilon_a \sigma_\nu^J\, h_{a\mu\nu k} \tag{6}$$

where we denote the spatial parameter for surface I as simply x with patch index I implied— x means x^I in a function defined on area A^I.

Let us call the shading, σ, and the interreflection parameters, β, *fields*, since they take on values throughout subspaces of the image. The question arises: how many fields and how many unknown parameters ϵ, σ can we expect to derive from the available ρ information? In [8] we showed that for just two patches, assuming the β^{11} approach zero far away from an edge we can find the fields β^{21} and β^{12} as well as all the ϵ_a, σ_a up to one overall multiplicative constant for all unknowns solved for, provided the dimensionalities of the finite-dimensional model spaces were related by $3s \geq 2n + m$.

In the present approach, the number of unknowns equals the number of values of all fields, plus the number of ϵ's and σ's, reduced by the number of constraints, if any, that can be applied amongst the fields and also reduced by 1 to account for one overall multiplicative constant. Such a constant arises because we cannot derive all values absolutely since, e.g., multiplying ϵ and all β's by a factor and dividing all σ's by the same factor results in the same measured values ρ. These unknowns must be balanced by the s values measured at each x for each of the M patches.

But not all the ρ information may be usable. E.g., for a single patch with no interreflection the number of observations may be sN, say, making measurements at N locations. But these measurements provide only $(s-1)+N$ independent values because all the ρ vectors are parallel. Therefore, besides scaling information we measure only a direction vector – there is not enough independent data to solve the problem.

In general we would make different numbers of observations in each patch. But for discussion purposes, suppose that we make N measurements of ρ in each patch. Then the number of measurements is sMN sensor values. The number of unknowns is given by the nM values of σ, the $m-1$ values of ϵ, setting one of the components of ϵ to 1 to pin down the arbitrary multiplicative constant, plus $MNF - C$ for all the values of F fields, say, that we wish to determine less C constraints that may obtain amongst them. Therefore we must have

$$nM + (m-1) + MNF - C \leq sMN$$

In general this inequation can be satisfied provided F is not chosen too large. However, in solving a set of equations for the unknowns one must check the rank of any matrix that is to be inverted in order to guard against degenerate data. This reflects the fact that given only a limited number of sensor classes, information that might be extracted in principle may be collapsed into too few measurements. As well, one must assess which interreflection effects can be expected to dominate in an image or else one will attribute values to one type of interreflection field that may actually be due to another.

3.4 Minimization integral

We take as a minimization integral the integral of the sum of squares of all the deviations of the measured ρ_k from the corresponding versions of the right-hand-side of eqn. (6). To simplify the resulting expression we adopt a modified form of the Einstein summation convention, whereby

summation is implied over repeated indices: we take repeated subscript indices to imply summation but assume that superscript indices are not summed over unless summation is explicitly shown.

With this convention, our minimization integral can be written

$$\Im \equiv \sum_I \int \left[\rho_k^I(x) - \alpha^I(x)\epsilon_a \sigma_\mu^I g_{a\mu k} - \sum_J \beta^{JI}(x)\sigma_\mu^I \epsilon_a \sigma_\nu^J h_{a\mu\nu k} \right]^2 dA^I \tag{7}$$

where $[\ ]^2$ is a shorthand for norm squared in s-dimensional space; e.g.,

$$[\rho_k]^2 \equiv \sum_k \rho_k \rho_k$$

We seek to minimize the above integral. Since α and β are functions, we can generate equations for them from this variational principle by taking variational derivatives of $\Im$. Solutions for such equations will be given as *algebraic* functions of ϵ and σ.

Let us assume for the present that all the functions β are independent. If this assumption is wrong it may be corrected by the addition of further terms to $\Im$. In Section 4 below we insert such constraints, based on knowledge of the physical meaning of β. We show there how such constraints modify the variational problem.

For each patch I and at each point x in the patch, we set the variational derivative with respect to α equal to zero (see, e.g., [3]):

$$\frac{\delta \Im}{\delta \alpha^I(x)} = -2 \left[\rho_k^I(x) - \alpha^I(x)\epsilon_a \sigma_\mu^I g_{a\mu k} - \sum_J \beta^{JI}(x)\sigma_\mu^I \epsilon_a \sigma_\nu^J h_{a\mu\nu k} \right] \left[\epsilon_b \sigma_\omega^I g_{b\omega k} \right] = 0 . \tag{8}$$

Viewing the above Euler-Lagrange equation as giving α in terms of all the other variables, we can immediately find the solution

$$\alpha^I(x) = \left\{ \left[\rho_k^I(x) - \sum_J \beta^{JI}(x)\sigma_\mu^I \epsilon_a \sigma_\nu^J h_{a\mu\nu k} \right] \left[\epsilon_b \sigma_\omega^I g_{b\omega k} \right] \right\} \Big/ \left\{ \left[\epsilon_b \sigma_\omega^I g_{b\omega k} \right]^2 \right\} . \tag{9}$$

The assumption built into the variational problem is that any observed ρ-vector is made up of a term proportional to illumination times reflectance, the primary component of the sensor values, plus terms corresponding to illumination times reflectance times an additional reflectance factor—the one-bounce components. Eqn. (9) states that the first of these, the no-bounce signal, has a shading factor α found by projection of the part of ρ not attributable to mutual illumination onto the no-bounce ρ-vector directions.

The similar variational derivatives for the β^{JI} give

$$\frac{\delta \Im}{\delta \beta^{JI}(x)} = -2 \left[\rho_k^I(x) - \alpha^I(x)\epsilon_a \sigma_\mu^I g_{a\mu k} - \sum_K \beta^{KI}(x)\sigma_\mu^I \epsilon_a \sigma_\nu^K h_{a\mu\nu k} \right] \left[\epsilon_b \sigma_\omega^I \sigma_\tau^J h_{b\omega\tau k} \right] = 0 . \tag{10}$$

This is a matrix equation for all the β^{JI} for a particular I, as can be seen by rewriting in the form

$$\left[\sum_K \beta^{KI}(x)\epsilon_a\sigma_\mu^I\sigma_\nu^K\, h_{a\mu\nu k}\right]\left[\epsilon_b\sigma_\omega^I\sigma_\tau^J\, h_{b\omega\tau k}\right] = \left[\rho_k^I(x) - \alpha^I(x)\epsilon_a\sigma_\mu^I\, g_{a\mu k}\right]\left[\epsilon_b\sigma_\omega^I\sigma_\tau^J\, h_{b\omega\tau k}\right]. \quad (11)$$

The β^{JI} are given in terms of projections of those parts of the ρ_k not accounted for by the primary color signal direction onto the one-bounce direction.

Taken together, eqns. (8) and (10) restate the major assumption that vectors ρ_k may be composed from a set of linearly independent vectors in the primary color signal ρ direction and in the set of one-bounce ρ directions. Any ρ is a projection onto these directions.

For the unknown constants ϵ_a and σ_μ^I, the minimization consists of an ordinary least-squares problem. Accordingly, we take partial derivatives of $\Im$. For the surface reflectance parameters σ we find

$$\frac{\partial\Im}{\partial\sigma_\mu^I} = -2\sum_J \int \left\{\left[\rho_k^J(x) - \alpha^J(x)\epsilon_a\sigma_\nu^J\, g_{a\nu k} - \sum_K \beta^{KJ}(x)\epsilon_a\sigma_\nu^J\sigma_\omega^K\, h_{a\nu\omega k}\right]\right.$$

$$\left.\left(\delta^{IJ}\left[\alpha^I\epsilon_b g_{b\mu k} + \sum_L \beta^{LI}\epsilon_b\sigma_\tau^L h_{b\mu\tau k}\right] + \left[\beta^{IJ}\epsilon_b\sigma_\tau^J h_{b\mu\tau k}\right]\right)\right\} dA^J = 0, \quad (12)$$

where δ^{IJ} is the Kronecker delta and equals 1 for $I = J$ and 0 otherwise. Note that the Ith term in the above sum is the most complex and also contributes the most to the sum. Both that term and the other terms contribute to the self-reflection from patch I onto itself. Eqns. (12) constitute M sets of n coupled equations in n unknowns for each patch.

The similar equations formed by taking partial derivatives with respect to the ϵ_a are

$$\frac{\partial\Im}{\partial\epsilon_a} = -2\sum_I \int \left\{\left[\rho_k^I(x) - \alpha^I(x)\epsilon_b\sigma_\mu^I\, g_{b\mu k} - \sum_K \beta^{KI}(x)\epsilon_b\sigma_\mu^I\sigma_\nu^K\, h_{b\mu\nu k}\right]\right.$$

$$\left.\left[\alpha^I\sigma_\omega^I g_{a\omega k} + \sum_L \beta^{LI}\sigma_\omega^L\sigma_\tau^I h_{a\omega\tau k}\right]\right\} dA^I = 0. \quad (13)$$

4 Simplified Configuration

In this section, we write out the above equations for the specialized situation of two convex patches illuminated by diffuse light. We see that the fields β^{12} and β^{21} are related by a reciprocity relation that leads to the necessity of adding an integral constraint term to the minimization integral.

4.1 Two convex patches, diffuse illumination

In the case of two surfaces only, with diffuse illumination and no point source, eqns. (8–13) are greatly simplified. Firstly, the shading field σ drops out because we examine an image formed by illumination with isotropic radiation. Since we also assume convex surfaces, the only one-bounce fields left are β^{12} and β^{21}.

For the special case we examine here, eqn. (11) becomes simply

$$\beta^{21}(x) = \left\{ \left[\rho_k^1(x) - \epsilon_a \sigma_\mu^1 g_{a\mu k} \right] \left[\epsilon_b \sigma_\nu^1 \sigma_\omega^2 h_{b\nu\omega k} \right] \right\} \Big/ \left\{ \left[\epsilon_d \sigma_\tau^1 \sigma_\kappa^2 h_{d\tau\kappa k} \right]^2 \right\} \tag{14}$$

and similarly for β^{12} with 1 exchanged everywhere with 2.

For σ_μ^1 eqns. (12) go over into the simpler form

$$\int \left[\rho_k^1(x^1) - \epsilon_a \sigma_\nu^1 g_{a\nu k} - \beta^{21}(x^1) \epsilon_a \sigma_\nu^1 \sigma_\omega^2 h_{a\nu\omega k} \right] \left[\epsilon_b g_{b\mu k} + \beta^{21}(x^1) \epsilon_b \sigma_\tau^2 h_{b\mu\tau k} \right] dA^1$$

$$+ \int \left[\rho_k^2(x^2) - \epsilon_a \sigma_\nu^2 g_{a\nu k} - \beta^{12}(x^2) \epsilon_a \sigma_\nu^1 \sigma_\omega^2 h_{a\nu\omega k} \right] \left[\beta^{12}(x^2) \epsilon_b \sigma_\tau^2 h_{b\mu\tau k} \right] dA^2 = 0 , \tag{15}$$

where now we show the index $I = 1$ or 2 on the set of parameters x^I that parameterize area A^I. The equations for σ_μ^2 are found by exchanging 1 with 2 in eqn. (15).

The ϵ_a equations, eqn. (13), become

$$\int \left[\rho_k^1(x^1) - \epsilon_b \sigma_\mu^1 g_{b\mu k} - \beta^{21}(x^1) \epsilon_b \sigma_\mu^1 \sigma_\nu^2 h_{b\mu\nu k} \right] \left[\sigma_\omega^1 g_{a\omega k} + \beta^{21}(x^1) \sigma_\omega^1 \sigma_\tau^2 h_{a\omega\tau k} \right] dA^1$$

$$+ \int \left[\rho_k^2(x^2) - \epsilon_b \sigma_\mu^2 g_{b\mu k} - \beta^{12}(x^2) \epsilon_b \sigma_\mu^1 \sigma_\nu^2 h_{b\mu\nu k} \right] \left[\sigma_\omega^2 g_{a\omega k} + \beta^{12}(x^2) \sigma_\omega^1 \sigma_\tau^2 h_{a\omega\tau k} \right] dA^2 = 0 . \tag{16}$$

Eqn. (14) states that once the ϵ_a, σ_μ^I are fixed, the interreflection factors are given algebraically: these factors follow from the component of the ρ_k not explained by the primary ρ that comes from the color signal.

Eqns. (15) and (16) are matrix equations. Eqn. (15) can be viewed as n equations in the n unknowns σ_μ^1. Similarly eqn. (16) is a set of m equations in the m unknowns ϵ_a.

In fact, to solve these equations given $\rho(x)$ (14) – (16) must be solved simultaneously. One then finds all the unknowns, β^{12}, β^{21}, ϵ_a, σ_μ^1, and σ_μ^2 such that all equations are satisfied.

4.2 Symmetry group

By inspection one sees that the above set of equations remains satisfied if one transforms one solution set into another by means of the transformation

$$\epsilon_a \to A \epsilon_a \; ; \; \sigma_\mu^1 \to \sigma_\mu^1 / A \; ; \; \sigma_\mu^2 \to \sigma_\mu^2 / A \; ; \; \beta^{21}(x^1) \to A \beta^{21}(x^1) \; ; \; \beta^{12}(x^2) \to A \beta^{12}(x^2) /; .$$

Since the above transformation constitutes a group, one may in principle be able to simplify the set of equations and even derive solutions by using group theory alone (see [5] and references cited therein).

For our current purposes, it is enough to note that one arbitrary multiplicative constant is available for scaling all the unknowns. We choose the scaling

$$\epsilon_1 \equiv 1 .$$

4.3 Dimensionalities

Inspection of eqn. (15) shows that as a matrix equation for σ^1 it can be rewritten as

$$\sigma^1_\nu L_{\nu k} M_{k\mu} = N_\mu$$

where L is an n by s matrix, M is an s by n matrix, and N is an 1 by n vector. Thus the matrix that must be inverted to solve for σ^1, *viz.* $L\,M$, can have at most rank s.

A similar statement can be made for eqn. (16). Since we wish to use an ordinary color camera with $s = 3$, in what follows we take

$$n = m = 3 .$$

Thus the present method does not allow higher dimensionalities than those arrived at in our previous work in [4].

4.4 Reciprocity constraint

By examining the exchange of power between patches, we showed in [8] that the one-bounce β^{21} can be identified with a *configuration factor* [24]. A configuration factor is a single-bounce, diffuse-reflector quantity describing the ratio of the power reaching a small area ΔA^1 from another surface A^2 normalized in terms of the total radiation leaving A^2. This factor incorporates all geometric factors— including view factors— and is integrated over all of area A^2. In [24] the configuration factor is denoted dF_{2-d1}, meaning that the configuration factor contains a differential and that it sums up the geometrical relationship between a finite area 2 and a differential area 1. Specifically, we showed that one could make the identification $dF_{2-d1} = \Delta A^1 \beta^{21}/A^2$.

Now from the reciprocity relation for configuration factors, $A^2 dF_{2-d1} = \Delta A^1 dF_{d1-2}$, we can in fact also make the identification $\beta^{21} = dF_{d1-2}$, where dF_{d1-2} gives the ratio of radiation leaving ΔA^1 that reaches $A2$, compared to all the radiation from ΔA^1 into the hemisphere above it.

Configuration factors can be summed into *form factors*, which express radiative exchange between finite surfaces: $F_{12} = (1/A^1) \int_{A^1} dF_{d1-2} dA^1$. A reciprocity relation exists between two form factors as well: $A^1 F_{1-2} = A^2 F_{2-1}$. Substituting the identification of β^{IJ}, we thus arrive at a constraint on values of β^{21} and β^{12} as follows:

$$\int_{A_1} \beta^{21}(x^1) dA^1 = \int_{A_2} \beta^{12}(x^2) dA^2 . \qquad (17)$$

This constraint can be added to our minimization problem as an integral constraint, with constant Lagrange multiplier Λ, via

$$\mathfrak{I} \rightarrow \mathfrak{I} - 2\Lambda \left(\int_{A_1} \beta^{21}(x^1) dA^1 - \int_{A_2} \beta^{12}(x^2) dA^2 \right) . \tag{18}$$

Equations for ϵ and σ are unaffected by this substitution, but eqn. (14) now becomes

$$\beta^{21}(x) = \left\{ \left[\Lambda + \rho^1_k(x) - \epsilon_a \sigma^1_\mu g_{a\mu k} \right] \left[\epsilon_b \sigma^1_\nu \sigma^2_\omega h_{b\nu\omega k} \right] \right\} \Big/ \left\{ \left[\epsilon_d \sigma^1_\tau \sigma^2_\kappa h_{d\tau\kappa k} \right]^2 \right\} \tag{14'}$$

The equation for β^{12} is similar, but with Λ replaced by $-\Lambda$.

Since Λ is a constant, we can solve for it. Substitution of (14′) into (17) gives the simple expression

$$\Lambda = \left\{ A^2 \left[\rho^2{}_k - \epsilon_a \sigma^2_\mu g_{a\mu k} \right] \left[\epsilon_b \sigma^1_\nu \sigma^2_\tau h_{b\nu\tau k} \right] - A^1 \left[\rho^1{}_k - \epsilon_a \sigma^1_\mu g_{a\mu k} \right] \left[\epsilon_b \sigma^1_\nu \sigma^2_\tau h_{b\nu\tau k} \right] \right\} / \left\{ A^1 + A^2 \right\} , \tag{19}$$

where ρ^l is the average of the vector ρ^l over A^l. This value of Λ must be substituted into eqn. (14′) whenever the β's are calculated.

For more than two patches, similar constraints occur for every patch pair.

4.5 Algorithm

In a similar fashion to our strategy in solving the nonlinear system of equations in [14, 9], we note that eqn. (15) is *linear* insofar as the vector σ^1 is concerned. Therefore we can solve for σ^1 provided all other variables are initialized. Similarly, eqn. (16) is linear in ϵ. Since by (14′) both functions β are given algebraically in terms of the measured ρ's and the variables ϵ and σ, an iterative solution is possible.

We found that the following scheme is satisfactory:

Initialize

Set $\vec{\epsilon} = (1,0,0)$.

Find the best first components of σ^1, σ^2 for measured ρ's via $\sigma^l_1 = [\rho^l \cdot \bar{\rho}^l]/[g_{11} \cdot \bar{\rho}^l]$, where $\bar{\rho}^l$ is the average of ρ^l over area A^l and g_{11} is the vector with components g_{11k}.

Find β^{21}, β^{12} via eqn. (14′).

While $\vec{\epsilon}$, $\vec{\sigma^1}$, $\vec{\sigma^2}$ not converged

/* Find those vectors $\vec{\epsilon}$, $\vec{\sigma^1}$, $\vec{\sigma^2}$ that are simultaneous solutions for eqns. (15), (16) for the current functions β^{21}, β^{12}. */

While $\vec{\epsilon}$, $\vec{\sigma^1}$, $\vec{\sigma^2}$ still changing

Solve eqns. (14′),(15) in turn for $\vec{\epsilon}$, $\vec{\sigma^1}$, $\vec{\sigma^2}$.

Find β^{21}, β^{12} via eqn. (14′).

4.6 Multiplicity of solutions

Since the set of equations (15), (16) is nonlinear, we can expect non-unique solutions. In particular while we are guaranteed that the integral 3 is being extremized, it may in fact be being maximized instead of minimized. For this reason, direct methods such as those in [1], which produce global minima, may be appropriate to the present problem.

We can think of eqns. (15),(16) as an algebraic problem to be solved using Cramer's rule, with the β^{IJ} substituted, in terms of ϵ and the σ's, from eqns. (14′). Using the dimensionalities stated above, suppose we were to first solve eqn. (15) for the σ^1-vector. Then we could substitute the resulting algebraic expression for σ^1 into the equations for σ_μ^2 and solve for the σ^2-vector. In terms of σ^2, β^{21} is a rational function with numerator of degree 1 and denominator of degree 2 while in terms of σ^1 it is a 2nd degree over a 2nd degree. As well, the solution of eqn. (15) for σ^1 is already a complex rational function of σ^2 even without including the nonlinearities in the β^{IJ}. Therefore the fully simplified version of an equation for component σ_μ^I will be a polynomial of fairly high degree. Multiple roots are to be expected.

We found that in tests using simulated edges (Section 5, below) the system of equations did indeed sometimes proceed to maximize the integral 3. Therefore we discard those solutions and change the initialization. As well, we also found solutions for which the recovered ϵ was far from the possible vectors associated with illumination vectors. These solutions we also discard. For each test we found only one solution that was not ruled out by these filtering criteria; the solutions retained were found to produce reasonable agreement with the correct data. The problem of multiplicity of solutions will be pursued in further work.

5 Simulations

We carried out a test of the model by simulating the edge depicted in Fig. 2. Here two semi-infinite flat planes of different widths and with different surface reflectance functions meet with opening angle γ. The field β^{21} takes into account all the reflection contributions from area A^2 to the small area ΔA^1. The complete infinite bounce color signal can be calculated for each side by using the radiosity method, but carrying out the infinite-bounce calculation separately for each wavelength instead of using only three color bands [4]. Sensor values ρ_k^I can then be calculated by integration with a set of filters. The result is that sensor values vary in a nonlinear fashion across each side and approach no-interreflection values far from the edge [4].

To test our method we carried out the above algorithm with a synthesized edge as input having $\gamma = 135°$ and surface 2 be twice the width of surface 1. As a first example, we consider an edge composed of two natural reflectance spectra drawn from the large catalogue [20] of measured data. In particular, we chose Krinov#54 (River valley with meadows) and Krinov#248 (Sand dunes) and illuminate the scene with standard illumination A [27]. Since we use Judd et al.'s daylight basis [16] and Cohen's Munsell chip basis [2], none of the spectral functions has anything to do with any

	Algorithm		Algorithm scaled		Best fit	
	$\mathcal{E}$ %	ΔE	$\mathcal{E}$ %	ΔE	$\mathcal{E}$ %	ΔE
Illumination	8.32	10.09	7.45	10.09	5.68	4.06
Reflectance 1	11.30	3.49	10.18	3.03	8.11	2.92
Reflectance 2	6.68	2.91	2.90	2.54	2.39	1.11

Table 1: Planar edge results, two natural reflectances illuminated by illuminant A.

of the basis sets.

As error measures for the illumination and the surface spectral reflectance functions we use the percentage error defined in [14], *viz.* $\mathcal{E} = \{\sum[f(\lambda) - \tilde{f}(\lambda)]^2 / \sum[f(\lambda)]^2\}^{1/2}$, where $\tilde{f}(\lambda)$ is a function that approximates $f(\lambda)$. We also use the CIELUV [27] color-difference formula ΔE. Here we use a 3-dimensional ΔE that measures changes in intensity as well as in chromaticity.

Table 1 shows the results for this test. The first two columns show the error measures for the illuminant spectrum recovered by our algorithm. Since we set $c_1 = 1$ the scaling for the spectrum is wrong, so we first scale the whole spectrum by the c_1 for a least-squares fit to the spectrum A using three basis vectors. The middle two columns are these same errors, but for approximating spectra that are scaled by a factor minimizing the error (see [14]). The middle columns are then a good test of color constancy without regard for intensity recovery. The right two columns show the errors for the best least-squares fit directly to each of the spectra using the finite-dimensional model.

As can be seen, the recovery algorithm does not add much error to that already caused by the finite-dimensional approximation. Fig. 3 shows how well these spectra fit the actual functions.

In Fig. 4 we show how well values of β match a theoretical calculation. Here we compare the recovered values of β, scaled up by c_1, with a theoretical function ζ calculated using one bounce [4]. In Fig. 2, $\zeta = 1/2[1 + (\cos\gamma - X)/(X^2 + 1 - 2X\cos\gamma)^{1/2}]$, where X is the dimensionless distance $X = x/\xi$. We can expect β to resemble this function, offset from its value far away from the edge, since β interprets multiple interreflections within a one-bounce model whereas the theoretical ζ is calculated for the case of exactly one bounce. Therefore we could expect β to be greater than ζ (see [4]); however, that is not the case here because the illumination and reflectances are not modeled exactly.

We see that the algorithm approximately recovers values that are offset with respect to the theoretical function. Using a similar "error" measure as the measure $\mathcal{E}$ that we used for spectra (although we do not expect β to match ζ exactly), we find $\mathcal{E} = 5.93\%$ on side 1 of the edge and $\mathcal{E} = 4.65\%$ on side 2. (These values can be reduced by scaling and offsetting via $\beta \rightarrow A\beta + B$.

	Algorithm		Algorithm –scaled		Best fit	
	$\mathcal{E}$ %	ΔE	$\mathcal{E}$ %	ΔE	$\mathcal{E}$ %	ΔE
Illumination	8.44	10.24	7.56	10.24	5.68	4.06
Reflectance 1	10.03	3.39	9.12	3.23	6.99	2.95
Reflectance 2	6.30	3.97	4.53	3.89	3.87	3.47

Table 2: Planar edge, natural reflectances, illuminant A; Krinov principal component basis.

Then $\mathcal{E}$ becomes 0.4% on both surfaces.)

If we change the basis sets we use for reflectance and illumination, we can expect to get somewhat different answers. In particular if we use a reflectance basis set that better models those reflectances we actually expect to see in an image then we might expect to do better. In Table 2 we show the results for the same reflectances as above, but using for reflectance basis functions a set of vectors derived from a principal component analysis we carried out on the complete set of over 300 Krinov spectra (cf. [21]). One would expect that when the basis functions are well-matched to reflectances expected in the image the algorithm would work better. However the basis functions, while explaining the variance for a large set of data, do not necessarily work well for any particular reflectance function. We see from Table 2 that while reflectance 1 is modeled slightly better by the Krinov basis, reflectance 2 is modeled slightly worse. The algorithm does a slightly poorer job of recovering the illumination spectrum, but improves on its estimates of the reflectance spectra. Note that the error measure ΔE is a nonlinear measure that does not necessarily strictly follow improvements in the error $\mathcal{E}$.

For the functions β, we find error values $\mathcal{E} = 5.97\%$ and $\mathcal{E} = 4.69\%$ on side 1 and side 2. For scaled curves these figures become 0.4% and 0.4%.

As another test, we measured the spectral reflectance functions of colored construction paper using a Zeiss RFC-3 Colorimeter (see [12]). This device gives spectrophotometric readings as well as chromaticities. Table 3 shows the results of applying our algorithm to the planar edge of Fig. 2 composed of pink and green paper illuminated by standard illuminant A. We used the Munsell chip basis for this test. We found that even though the green paper is very poorly modeled by this basis, the algorithm still does reasonably well in recovering the spectra that are better modeled. Also, the recovery of the β functions was about the same in all the tests we carried out.

For the β's, values of $\mathcal{E}$ found were $\mathcal{E} = 4.43\%$ and $\mathcal{E} = 9.85\%$. Errors for scaled curves were 2.0% and 0.3%.

	Algorithm		Algorithm scaled		Best fit	
	$\mathcal{E}$ %	ΔE	$\mathcal{E}$ %	ΔE	$\mathcal{E}$ %	ΔE
Illumination	10.56	13.26	9.23	13.26	5.68	4.06
Pink	20.06	13.84	14.52	13.18	10.56	5.12
Green	33.07	29.95	30.72	30.73	21.08	8.18

Table 3: Planar edge, construction paper, illuminant A; Munsell principal component basis.

6 Conclusions

This work points out the usefulness of color in determining shading and interreflection fields: simply measuring grey levels would not produce sufficient information to allow direct determination of these fields. The method produces estimates for the surface and illuminant spectra and for the shading and interreflection fields. Since the surface spectral reflectance is determined without advance knowledge of the ambient illumination, the method provides color constancy.

Allowing each spectrum to be scaled independently produces better results for the reflectance and illumination spectra, so the algorithm does better in determining color than absolute brightness. Nevertheless, the interreflection fields found are quite accurate even with respect to absolute scaling, although it is necessary to shift the origin by an offset.

Since the algorithm recovers offset versions of the interreflection functions β, the method could benefit from the addition of further constraints based on the positivity of these functions and of the shading functions α (see [18]).

More tests of the method are certainly in order. Without including shading, one could consider interreflections among more patches. As we increase the number of patches, we can expect the accuracy of estimation of $E(\lambda)$ to increase since more patches would provide further constraints upon it. Shaded surfaces and self-reflecting surfaces also need to be tested. Tests of real images of three-dimensional models, while difficult to carry out because of the necessity of careful calibration, will be pursued.

The strength of the variational approach to mutual illumination in color images is its potential generality, as seen in Section 3. The advantage of analyzing color images instead of grey-level images lies in the fact that color provides extra constraints that allow the mutual illumination effects to be interpreted properly.

7 Acknowledgements

M.S. Drew is indebted to the Centre for Systems Science at Simon Fraser University for partial support; B.V. Funt thanks both the CSS and the Natural Sciences and Engineering Research Council of Canada for their support.

8 Figure captions

Figure 1. Each point on a surface has a shading factor that depends on the local normal $\hat{n}$. Taking into account one interreflection bounce only, a point on surface 1 receives light reflected from all of surface 1 that is proportional to β^{11} and from all of surface 2 that is proportional to β^{21}.

Figure 2. For planar surfaces under diffuse illumination there is no shading factor or self-reflection. The amount of light reflected from all of a semi-infinite surface A^2 onto a small area ΔA^1 of a semi-infinite surface A^1 depends only on the distance x of the spot ΔA^1 from the edge compared to the width ξ of A^2.

Figure 3. Recovered spectra for illumination and the two surface reflectances for the planar edge of Fig. 2. Error data is given in Table 1. Shown are the actual spectrum (——), the recovered spectrum including brightness information ( ), the recovered spectrum scaled to give the best match to the actual spectrum (— — —), and the best fit available within a finite dimensional model of dimension 3 (···).

Figure 4. Interreflection factors recovered by the algorithm are shown for the planar edge of Fig. 2, with the width of surface 2 equal to twice the width of surface 1. The algorithm recovers the function β. On surface 1 this is β^{21} and on surface 2 it is β^{12}. For comparison we show the factor ζ derived from theory for a single bounce. The curves for β and ζ agree well once both curves are offset such that they both go to zero at the pixel farthest from the edge.

References

[1] A.A. Amini, T.E. Weymouth, and R.C. Jain. Using dynamic programming for solving variational problems in vision. *IEEE Trans. Patt. Anal. and Mach. Intell.*, 12:855–867, 1990.

[2] J. Cohen. Dependency of the spectral reflectance curves of the Munsell color chips. *Psychon. Sci.*, 1:369–370, 1964.

[3] R Courant and D. Hilbert. *Methods of Mathematical Physics.* Interscience Publishers, 1962.

[4] M.S. Drew and B.V. Funt. Calculating surface reflectance using a single-bounce model of mutual reflection. In *Proceedings: International Conference on Computer Vision, Osaka, Dec.4-7/90.* IEEE, 1990.

[5] M.S. Drew, S. Kloster, and J.D. Gegenberg. Lie group analysis and similarity solutions for the generalized liouville equation. *Nonlinear Analysis, Theory, Methods & Applications*, 13:489 505, 1989.

[6] D. Forsyth and A. Zisserman. Mutual illumination. In *Proceedings: Computer Vision and Pattern Recognition*, pages 466–473. IEEE, 1989.

[7] D. Forsyth and A. Zisserman. Shape from shading in the light of mutual illumination. *Image and Vision Computing*, 8:42–49, 1990.

[8] B.V. Funt, M.S. Drew, , and J. Ho. Color constancy from mutual reflection. Technical Report CSS/LCCR TR 89-02, Simon Fraser University School of Computing Science, 1989.

[9] B.V. Funt, J. Ho, and M.S. Drew. Method and apparatus for determining ambient light and surface reflectance. United States Patent Pending, 1988.

[10] R. Gershon, A.D. Jepson, , and J.K. Tsotsos. Ambient illumination and the determination of material changes. *J. Opt. Soc. Am. A*, 3:1700–1707, 1986.

[11] C.M. Goral, K.E. Torrance, D.P. Greenberg, and B. Battaile. Modeling the interaction of light between diffuse surfaces. *Computer Graphics*, 18:213–222, 1984.

[12] F. Grum and C.J. Bartleson. *Color Measurement*, volume 2 of *Optical Radiation Measurements.* Academic, 1980.

[13] R. Hall. *Illumination and color in computer generated imagery.* Springer-Verlag, New York, 1989.

[14] J. Ho, B.V. Funt, and M.S. Drew. Separating a color signal into illumination and surface reflectance components: Theory and applications. *IEEE Trans. Patt. Anal. and Mach. Intell.*, 12:966–977, 1990.

[15] B.K.P. Horn. Understanding image intensities. *Artif. Intell.*, 8:201–231, 1977.

[16] D.B. Judd, D.L. MacAdam, and G. Wyszecki. Spectral distribution of typical daylight as a function of correlated color temperature. *J. Opt. Soc. Am.*, 54:1031–1040, August 1964.

[17] J.E. Kaufman. *IES Lighting Handbook.* Illuminating Engineering Society, 4th edition, 1966.

[18] S. Kawata, K. Sasaki, and S. Minami. Component analysis of spatial and spectral patterns in multispectral images. i. basis. *J. Opt. Soc. Am. A*, 4:2101–2106, 1987.

[19] J.J. Koenderink and A.J. van Doorn. Geometrical modes as a general method to treat diffuse interreflections in radiometry. *J. Opt. Soc. Am.*, 73:843–850, 1983.

[20] E.L. Krinov. Spectral reflectance properties of natural formations. *Technical Translation TT-439, National Research Council of Canada*, 1947.

[21] L.T. Maloney. Evaluation of linear models of surface spectral reflectance with small numbers of parameters. *J. Opt. Soc. Am. A*, 3:1673–1683, 1986.

[22] L.T. Maloney and B.A. Wandell. Color constancy: a method for recovering surface spectral reflectance. *J. Opt. Soc. Am. A*, 3:29–33, 1986.

[23] S.K. Nayar, K. Ikeuchi, and T. Kanade. Shape from interreflections. Technical Report CMU-RI-TR-90-14, Robotics Institute, Carnegie Mellon University, 1990. To be presented at ICCV'90.

[24] R. Siegel and J.R. Howell. *Thermal Radiation Heat Transfer.* Hemisphere Pub. Corp., 1981.

[25] E.M. Sparrow and R.D. Cess. *Thermal Radiation Heat Transfer.* Hemisphere Pub. Corp., 1978.

[26] B.A. Wandell. The synthesis and analysis of color images. *IEEE Trans. Patt. Anal. and Mach. Intell.*, PAMI-9:2–13, 1987.

[27] G. Wyszecki and W.S. Stiles. *Color Science: Concepts and Methods, Quantitative Data and Formulas.* Wiley, New York, 2nd edition, 1982.

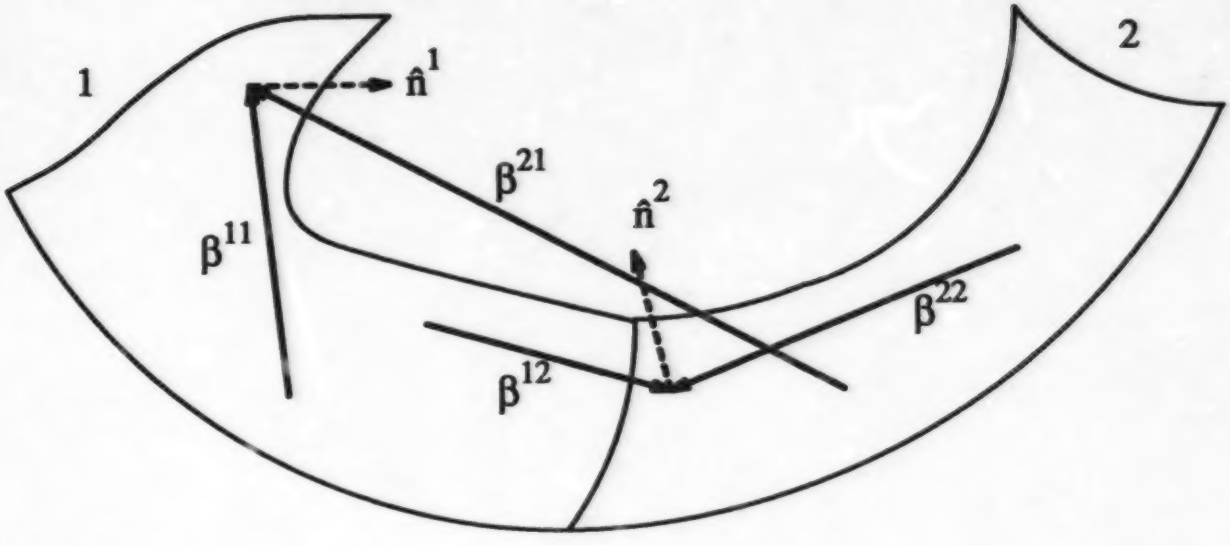

Fig. 1

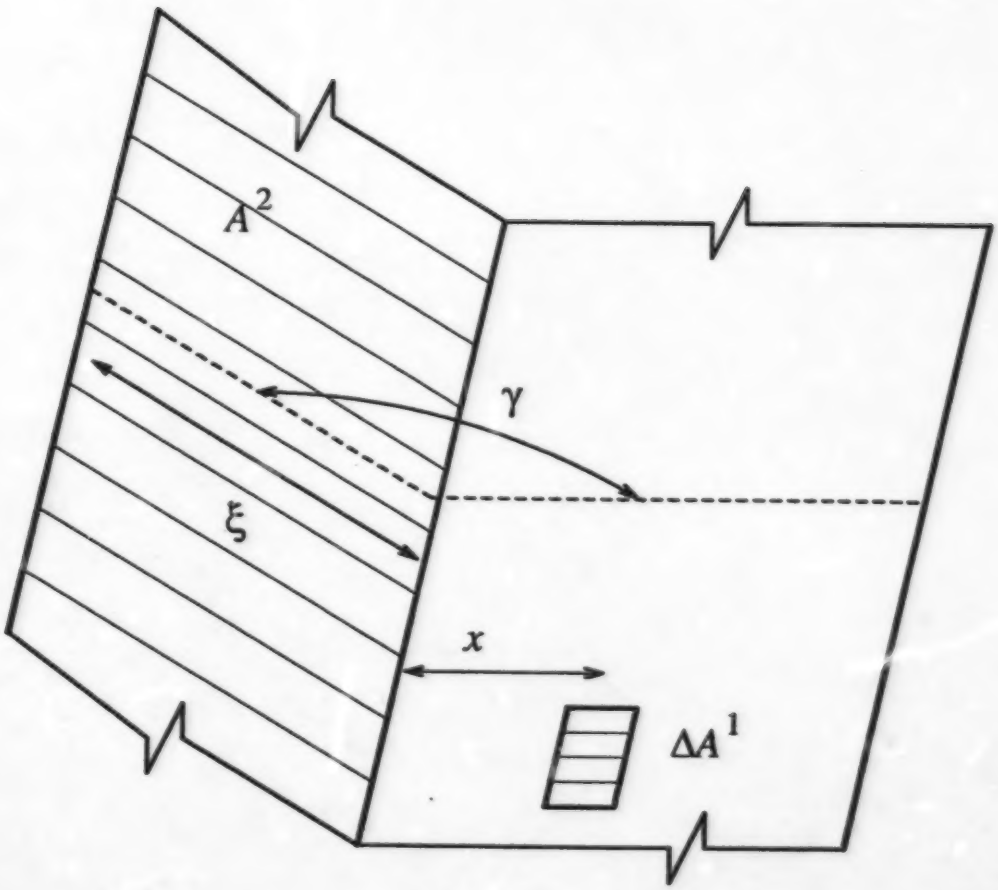

Fig. 2

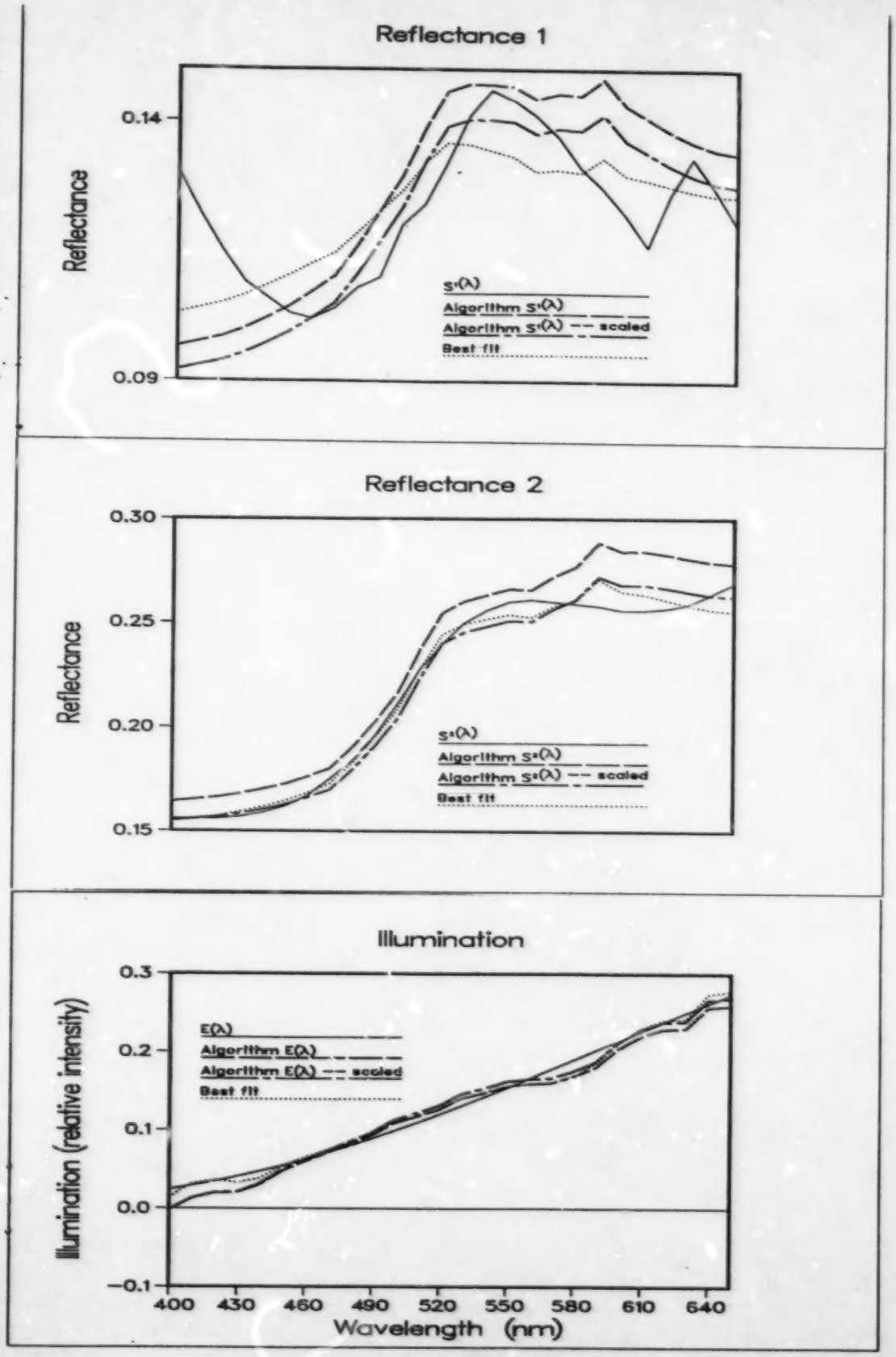
Reflectance 1
Reflectance
0.14
0.09
S¹(λ)
Algorithm S¹(λ)
Algorithm S¹(λ) -- scaled
Best fit
Reflectance 2
Reflectance
0.30
0.25
0.20
0.15
S²(λ)
Algorithm S²(λ)
Algorithm S²(λ) -- scaled
Best fit
Illumination
Illumination (relative intensity)
0.3
0.2
0.1
0.0
−0.1
E(λ)
Algorithm E(λ)
Algorithm E(λ) -- scaled
Best fit
400 430 460 490 520 550 580 610 640
Wavelength (nm)

Fig. 3

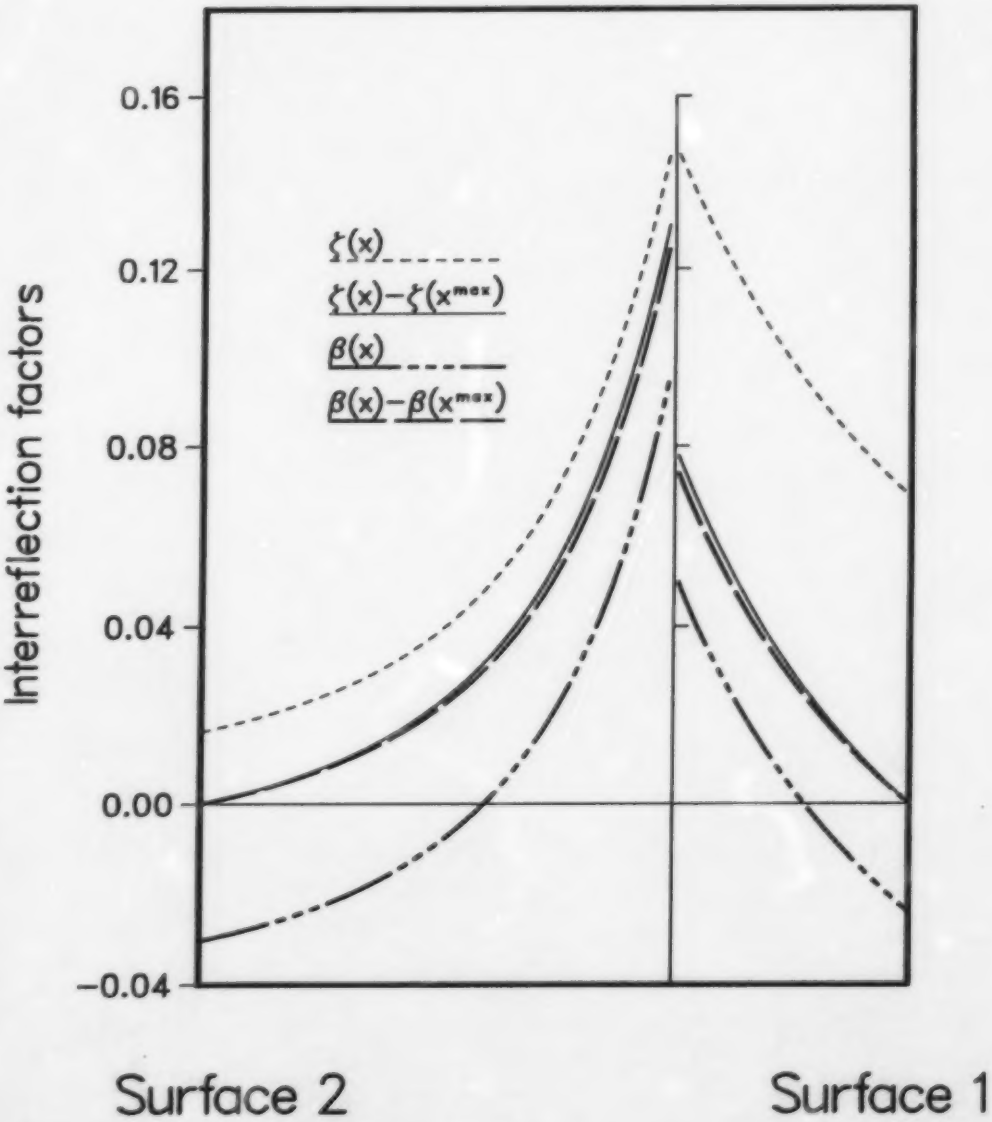
0.16
0.12
0.08
0.04
0.00
−0.04
Interreflection factors
ζ(x)
ζ(x)−ζ(x^max)
β(x)
β(x)−β(x^max)
Surface 2
Surface 1

Fig. 4

Centre for Systems Science

• Simon Fraser University established the **Centre for Systems Science** as a provincial centre for advanced study. The objective of CSS is twofold: coordinate and combine advanced systems research at SFU, and encourage application of research results within industry in order to further the technological development of British Columbia.

• CSS has assembled three research groups to streamline its efforts. The orientation of these groups is as follows: intelligent systems, microelectronics, and computer and communications systems. Because of shared research interests, this latter group merges with LCCR (**Laboratory for Computer and Communications Research**) for the publication of technical reports.

• CSS's three groups involve over 80 skilled faculty researchers principally from SFU's Schools of Engineering Science and Computing Science, but also draw substantially on Mathematics, Physics, Geography, Philosophy, Linguistics, Psychology, Communication, and Kinesiology.